Iranian Journal of Geophysics, Vol 17 No 3, 2023, Page 27 – 44 (Research Article)
DOI: 10.30499/IJG.2023.361202.1453

Geoelectrical Characterization of the Peat Soil at Klias Peninsula, Beaufort, Sabah (Malaysia)

Zamri Syarifah Nurmaisarah[1], Musta Baba[1], Habib Musa Mohamad[2] and Saleh Hardianshah[1*]

[1] *Program of Geology, Faculty of Science and Natural Resources, University Malaysia Sabah, Sabah, Malaysia*
[2]*Faculty of Engineering, University Malaysia Sabah, 88400 Kota Kinabalu, Sabah, Malaysia*

(Received: 08 September 2022, Accepted: 25 January 2023)

Abstract

Electrical resistivity imaging (ERI) surveys were carried out at the Klias Forest Reserve, Beaufort, Sabah. The entire area consists of Crocker Formation and Quaternary deposits. The main purpose of the geophysical surveys was to characterize the properties of peat and measure the thickness of the peat soil. For this purpose, seven (7) traverses were established for electrical resistivity imaging (ERI) and induced polarization imaging (IPI). The configuration of the Schlumberger and Wenner array was applied by adopting 41 electrodes with 1.0m-5.0m electrode spacing. The length of the ERI & IPI survey line varies from 80m- 200m. The core samples were collected at a depth of 0-6m. The resistivity survey lines R1, R2, R3, and R4 were conducted nearby Borehole A. Borehole B was taken alongside the survey line R5. Whereas Borehole C was taken near survey lines R6 and R7. The results of the ERI & IPI surveys show that the subsurface strata are composed of peat materials with resistivity values of 15Ωm – 500 Ωm, clay having resistivity values of 30 Ωm – 60 Ωm and resistivity value of boundary between peat and marine clay resistivity range from 20 Ωm -80 Ωm. The thickness of the peat and clay obtained ranges from 0-6m and 6m-28m respectively. The clay layer is thickening towards the West to the East. While the peat layer shows a varied pattern from West to East. The combined approach between ERI, IPI and core sampling helped to better define the characterization of the material and their thicknesses within the subsurface.

Keywords: Resistivity, Induced Polarization, Geophysics, Peat Soil

*Corresponding author: hardianshah@ums.edu.my

1 Introduction

Tropical peat is formed by the accumulation of organic matter composed of undecomposed dead vegetation materials due to waterlogging (Jaenicke et al., 2008). Saturated peat retains a high water content ranging from 100% to 1000%, which slows the decomposition rate of organic matter and increases the thickness of the peat (Yusa et al., 2019). The decomposition rate of organic matter is influenced by the fluctuation of the water table. Drained peat leads to the depletion of the groundwater table, thus plenty of oxygen-filled space above the water table which activates microbial activities (Gusti et al., 2021). The rapid decomposition process is caused by the breakdown of phenolic compounds under aerobic conditions (Yule et al., 2016, 2018), hence increasing the CO_2 released by the oxidation process. As a result, fluctuation of the water table may affect the accumulation of organic content, peat thickness and carbon loss to the atmosphere.

2D Electrical resistivity imaging (ERI) is a geophysical technique for imaging subsurface properties based on electrical resistivity measurements via multi-electrode configuration. The resistivity value was able to be determined by making the measurements of potential differences at different potential electrodes, converting these values into apparent resistivity then inverting the data set (Loke et al., 2011; Saleh and Samsudin, 2013a,b). Whilst the peat soil is chargeable, the induced polarization imaging (IPI) method is used as a complementary method for defining peat thickness (Lee and Andrew, 2002). The combined approach between IPI, ERI, core sample and the stratigraphic information can produce detailed subsurface of the peat deposits (Pezdir et al., 2021). The selection of optimum electrode array configuration is important to determine the effectiveness and robustness of ERI results (Ishola et al., 2014). The Schlumberger and Dipole-Dipole arrays are widely used in subsurface electrical surveys. Each array provides a variety of geometric factors and sensitivity (Loke et al., 2013; Saleh and Samsudin, 2014). The Wenner array is much less noise-sensitive and better at resolving vertical changes while reaching shallower depths (Ishola et al., 2021).

In terms of geophysics, typical peat soil resistivity values range from 41 Ωm to 130 Ωm (Kowalczyk et al., 2017; Basri et al., 2019; Pezdir et al., 2021; Yusa et al., 2021). According to Yusa et al. (2019), resistivity values decrease with depth. The previous research (Erica et al., 2020) revealed peatland stratigraphy lie on peat and marine clay layers. Based on Ishola et al. (2021), the resistivity value obtained for the subsurface strata of peat and organic materials is 0.7 Ωm to 3 Ωm and resistivity value of clay layer is 5 Ωm to 50 Ωm. The values were mapped at different depths. Variations of materials in the subsurface affect the resistivity value. According to Dahlin and Zhou (2006), electrical resistivity is a physical characteristic of the subsurface that relies on porosity, grain cementation, compactness, water content, mineral composition, and clay mineral. Furthermore, the electrical resistivity of peat depends on organic content, mineral composition, moisture content, and water conductivity in peat pores (Kowalczyk et al., 2017; Yusa et al., 2019; Muhammad et al., 2020).

Higher resistivity values were obtained on the peat soil layer compared to the marine clay layer (Mohamad et al., 2021). The low resistivity value in marine clay was influenced by the clay particles which facilitate the surface conductance of electric current. Furthermore, the low resistivity value of marine clay is altered by the salt content in pore fluid-induced electrical conductivity (Long et al., 2012). The resistivity value for marine clay ranges from 5 Ωm to 150 Ωm. The minimum resistivity for marine clay was 8 Ωm with the salt content increased to 7 g/L (Tao et al., 2018).

In this paper, we present the results obtained by using ERI for resolving the thickness of the peat. The main advantage of this method is to obtain data on the peat-clay boundary and to determine the stratigraphy below the peat layer in the soil profile.

2 Materials and methods

2-1 Site selection

The study site is the Klias Peninsula, Beaufort, Sabah which is located at the South-West Sabah by latitude 5°17'3"N to 5°22'3"N and longitude 115°39'06"E to 115°43'03"E (Fig. 1). The area is characterized by Crocker Formation and alluvium deposits with a coastal geomorphological area reaching an elevation of 10-180 m. The elevation gradually lowers towards the western direction. The climatic condition is moderately humid and receives high annual rainfall between 2500 mm to 3000 mm in October-December (>300 mm) (Phua et al., 2008).

A sequence of peat and marine clay was observed in the underlying strata (Zamri et al., 2022).

2-2 Borehole sampling

Three borehole stations were produced with depths up to 6 m to acquire in-situ soil profile and thickness information within each of the resistivity survey lines. Peat soil samples were collected as undisturbed samples by using a pit sampler (6 m) and PVC (1 m) (Fig. 2). The resistivity survey lines R1, R2, R3, and R4 were conducted nearby Borehole A. Borehole B is taken alongside the survey line R5 whereas Borehole C is taken near to survey lines R6 and R7 (Fig. 1).

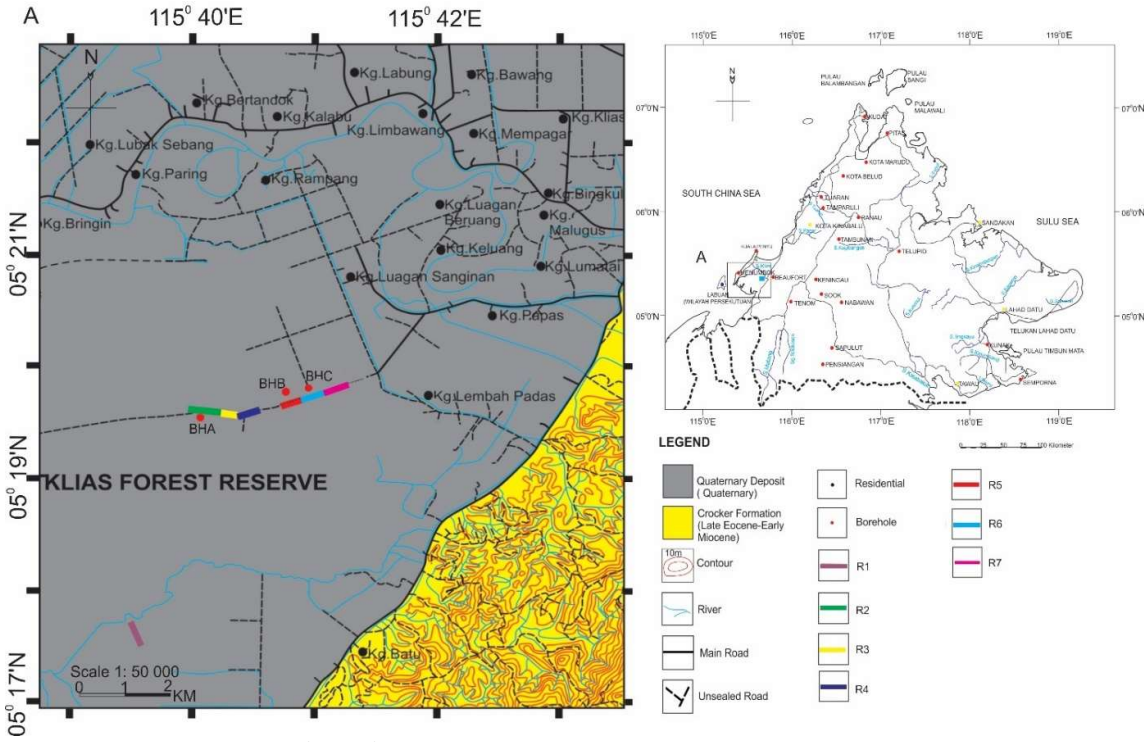

Figure 1. The geological map at Klias Forest Reserve, Sabah.

Figure 2. The peat soil sampling at Klias Forest Reserve, Sabah.

2-3 Electrical resistivity imaging (ERI) and Induced Polarization

In total, seven ERI & IPI surveys were conducted in the research area by using ABEM Terrameter LS. ERI & IPI is acquired by adopting 41 electrodes with 1.0-5.0 m electrode spacing and a total length varying from 80 m to 200 m. It was placed into the ground surface in a straight line. The availability of two cables with a 5 m electrode spacing was conducted to obtain the depth of prospection. The current was injected into the ground via stainless steel electrodes connected via multicable wire to the main computer unit to calculate and record the resistivity values and chargeability (for IPI) (Loke et al., 2003). The Wenner-Schlumberger configuration is used in the survey lines to obtain better depth investigation, lateral and vertical resolution, and noise sensitivity (Oktanius et al., 2016). Moreover, the survey line in this research only focuses on a particular area; thus, the roll-along technique is not applied.

The measurements were measured by flowing the electrical current into the ground through two current electrodes and measuring the differences in voltage at two potential electrodes. The electrode arrangement defines the resolution and depth of the soil. The bad data points with relatively low or high apparent resistivity values in the raw dataset were removed and processed using Res2DInv software (Bing and Torleif, 2003). The inversion modelling was carried out to produce the subsurface model (Loke et al., 2017). The number of iterations in the inversion process was repeated until the Root Mean Square (RMS) error fell below the acceptable target convergence of 5-10%. Finally, the interpretation of the ERI results was performed based on the correlation of the obtained inversion modelling (subsurface model) with the in-situ data (boreholes and outcrops).

3 Results

The selected peat profiles and their interpretation are presented in Figs. 3-9. Based on the resistivity models obtained, two types of distinct layers were recognized and classified as low resistivity (3-60 Ωm), intermediate resistivity (20-80 Ωm) and high resistivity (60-500 Ωm). By using core sampling, the peat soil profile revealed that these layers were separated by a layer of clay. Based on the borehole data, the boundary between peat and marine clay is found at a depth of 5.5 m with a resistivity value of 20-80 Ωm. Peat is present to a depth of 5 m and clay dominates at a depth of 6 m. For all resistivity sections, the first layer represents peat characterized by high resistivity value ranging from 15 Ωm to 500 Ωm and thickness of 0-5.5 m. It follows by a layer with low resistivity value ranging from 3 Ωm to 60 Ωm and thickness of 6-28 m consisting predominantly of clay.

Table 1. Electrical resistivity and thickness of peat soil profile at Klias Peninsula.

Configuration	ResistivityLine	Resistivity (Ωm)	Thickness (m)	Depth (m)	Soil Profile
Wenner	R1	40-500	5.5	0-5.5m	Peat
		30-80	2.5	5.5m-8m	Peat/Clay
		30-60	28	8m-36m	Clay
	R2	15-500	5.5	0-5.5m	Peat
		40-60	2.5	5.5m-8m	Peat/Clay
		10-60	6	8m-14m	Clay
	R3	60-400	5.5	0-5.5m	Peat
		10-60	8	5.5m-14m	Clay
Schlumberger	R4	40-500	5.5	0-5.5m	Peat
		30-70	2.5	5.5m-8m	Peat/Clay
		3-30	6	8m-14m	Clay
	R5	40-400	5.5	0-5.5m	Peat
		30-80	2.5	5.5m-8m	Peat/Clay
		10-60	28	8m-36m	Clay
	R6	40-400	5.5	0-5.5m	Peat
		20-60	2.5	5.5m-8m	Peat/Clay
		3-60	28	8m-36m	Clay
	R7	40-500	5.5	0-6m	Peat
		30-70	2.5	5.5m-8m	Peat/Clay
		15-60	28	8m-36m	Clay

3-1 Geoelectrical survey

Resistivity lines 1 to 7 cover a total line of 80-200 m with an electrode spacing of 1-5 m with a maximum depth of 14-36 m. The resistivity value ranges from 3 Ωm to 500 Ωm with an RMS error of 2-5% comprised of three major layers. The first layer indicates the peat layer with a resistivity value ranging from 30 Ωm to 400 Ωm at depth 0-6 m. The second layer represents a transition zone of peat and clay with a resistivity value ranging from 10 Ωm to 80 Ωm at depth 6-8 m. The third layer with a resistivity value ranging from 3 Ωm to 60 Ωm at depth 8-36 m was interpreted as a clay layer at depth of about 8m downwards.

Clay layers were detected at a saturated zone at depth of 6-8 m onwards from the surface. The appearance of clay shows a slightly higher IP reading ranging from 0.5 msec to 20 msec compared to the area within the subsurface (Figs. 3b-9b). The peat layer indicated by ranging from 1 msec to 7 msec with 0.84-39.0% RMS error, lies at the saturated zone at depth 0.5 m to 6 m. Based on the illustration (Figs. 3c-9c), the thickness of the peat layer is 5.5 m to 6 m. The transition zone of peat/clay which is between depths of 6 m to 8 m, is followed by the clay layer onwards.

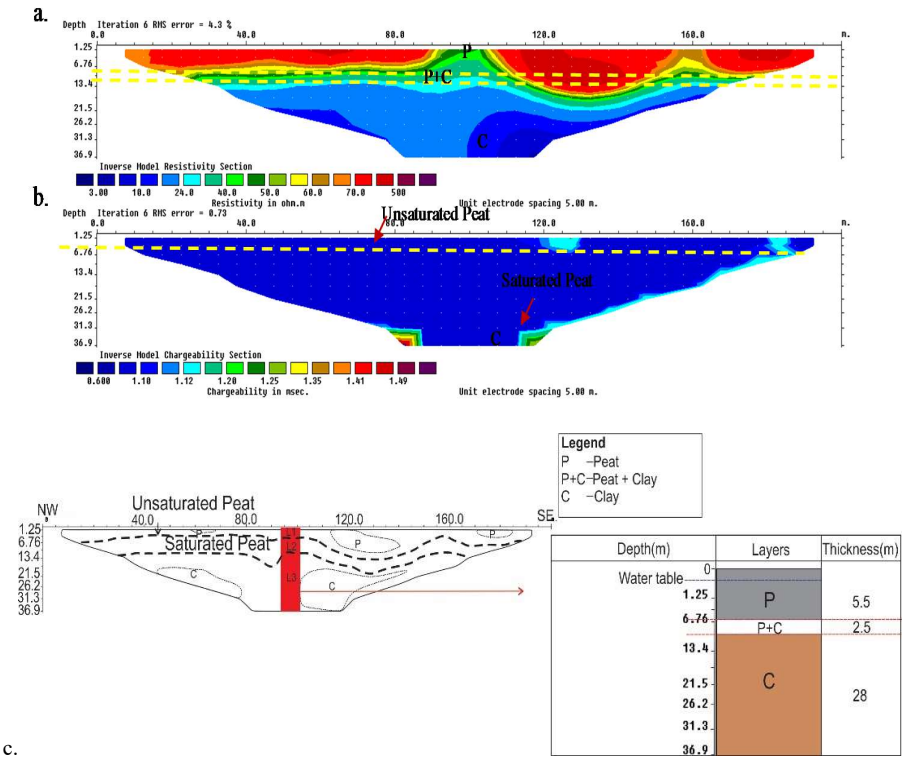
a.
b.
Unsaturated Peat
Saturated Peat
Legend
P –Peat
P+C–Peat + Clay
C –Clay
NW
SE
Depth(m)
Layers
Thickness(m)
Water table
P
P+C
C
5.5
2.5
28

c.

4

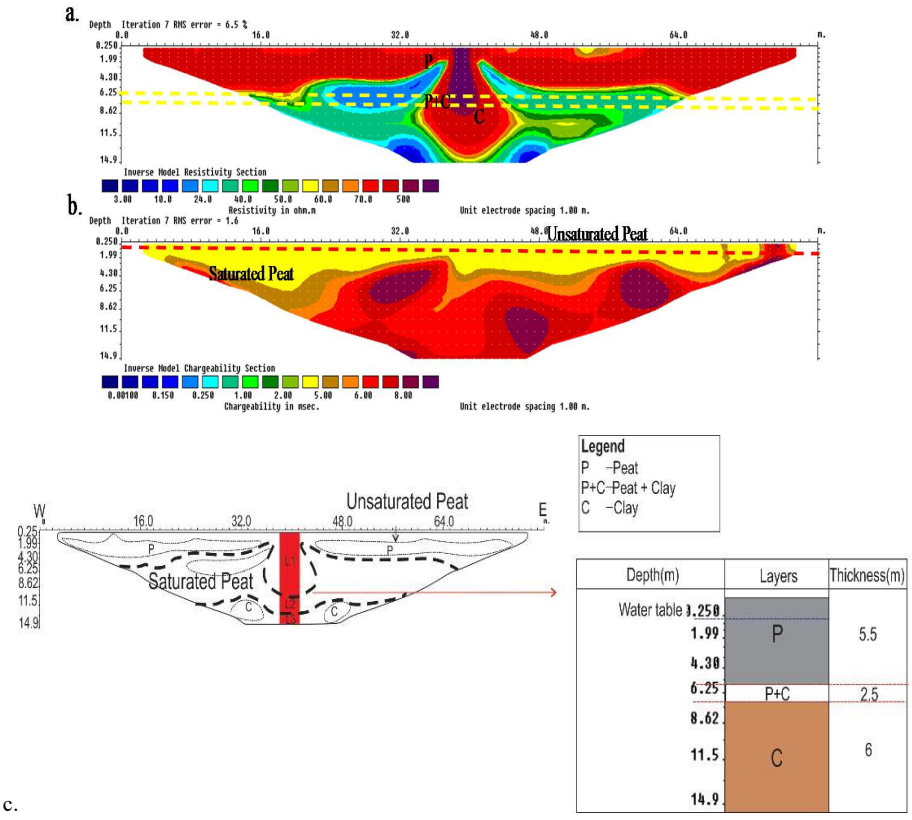
a.
b.
Unsaturated Peat
Saturated Peat
Legend
P –Peat
P+C–Peat + Clay
C –Clay
W
E
Depth(m)
Layers
Thickness(m)
Water table
P
P+C
C
5.5
2.5
6

c.

5

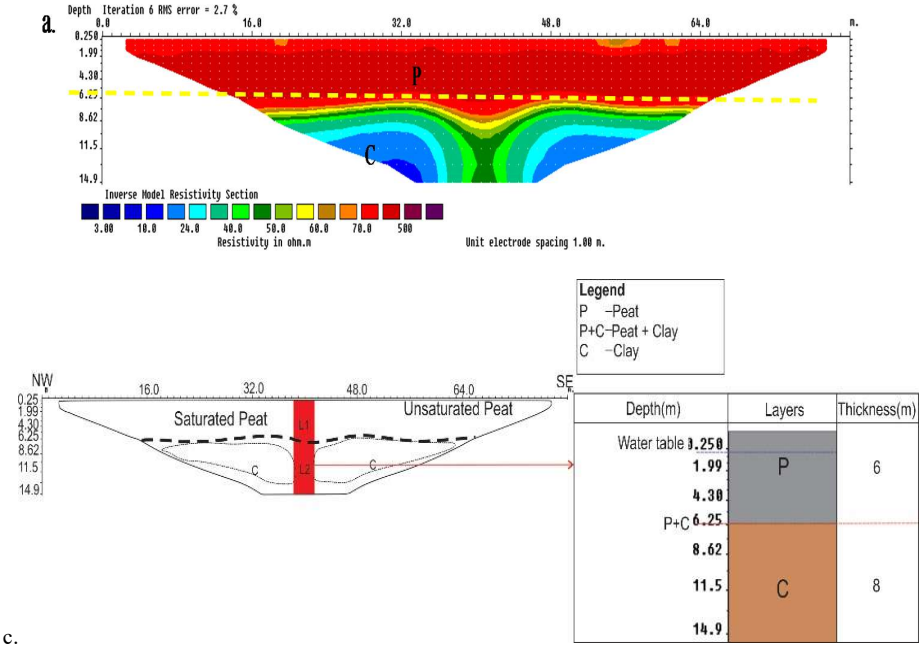
a.
Depth Iteration 6 RMS error = 2.7 %
P
C
Inverse Model Resistivity Section
Resistivity in ohm.m
Unit electrode spacing 1.00 m.
Legend
P –Peat
P+C–Peat + Clay
C –Clay
NW
SE
Saturated Peat
Unsaturated Peat
L1
L2
Depth(m)
Layers
Thickness(m)
Water table 3.250
1.99
4.30
P+C 6.25
8.62
11.5
14.9
P
C
6
8

c.

6

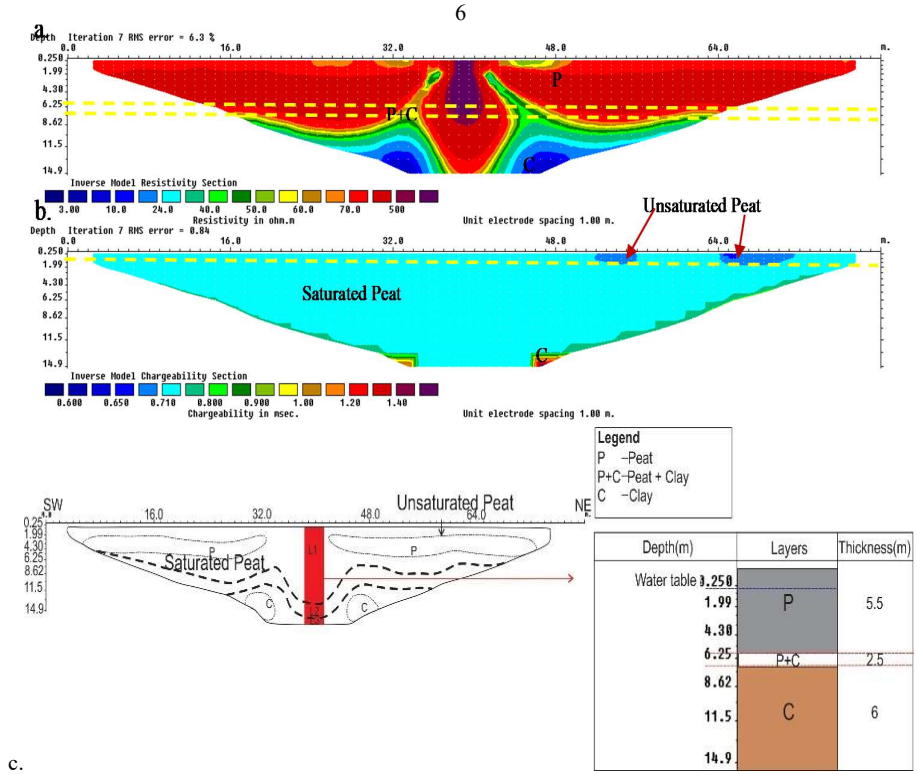
a.
Depth Iteration 7 RMS error = 6.3 %
P
P+C
C
Inverse Model Resistivity Section
Resistivity in ohm.m
Unit electrode spacing 1.00 m.
b.
Depth Iteration 7 RMS error = 0.84
Unsaturated Peat
Saturated Peat
C
Inverse Model Chargeability Section
Chargeability in msec.
Unit electrode spacing 1.00 m.
Legend
P –Peat
P+C–Peat + Clay
C –Clay
SW
NE
Unsaturated Peat
Saturated Peat
L1
L2
Depth(m)
Layers
Thickness(m)
Water table 3.250
1.99
4.30
6.25
P+C
8.62
11.5
14.9
P
C
5.5
2.5
6

c.

7

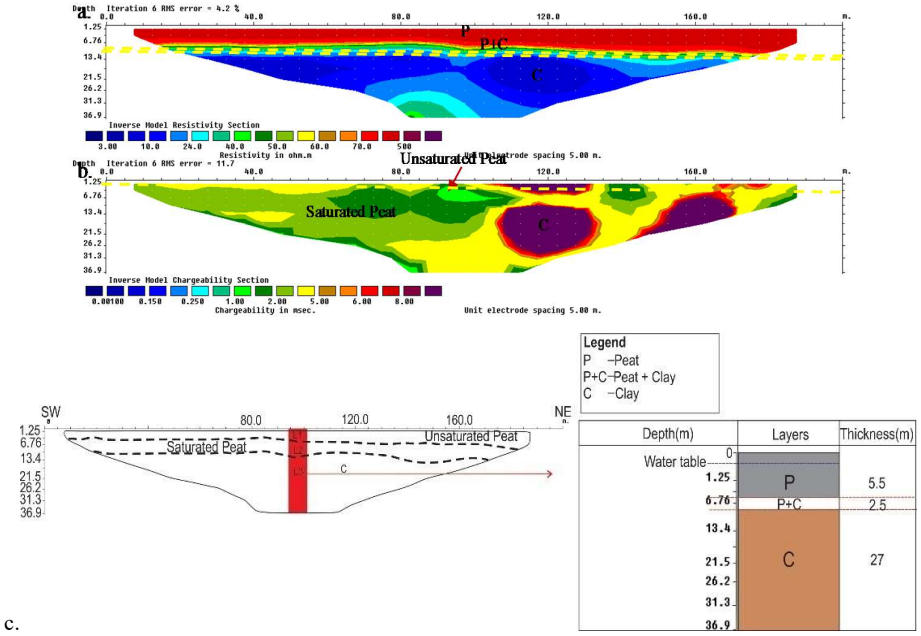
a.
P
P+C
C
Inverse Model Resistivity Section
Resistivity in ohm.m
Unit electrode spacing 5.00 m.
b.
Unsaturated Peat
Saturated Peat
C
Inverse Model Chargeability Section
Chargeability in msec.
Unit electrode spacing 5.00 m.
c.
SW
NE
Saturated Peat
Unsaturated Peat
C
Legend
P –Peat
P+C–Peat + Clay
C –Clay
Depth(m)
Layers
Thickness(m)
Water table
P
P+C
C
5.5
2.5
27

8

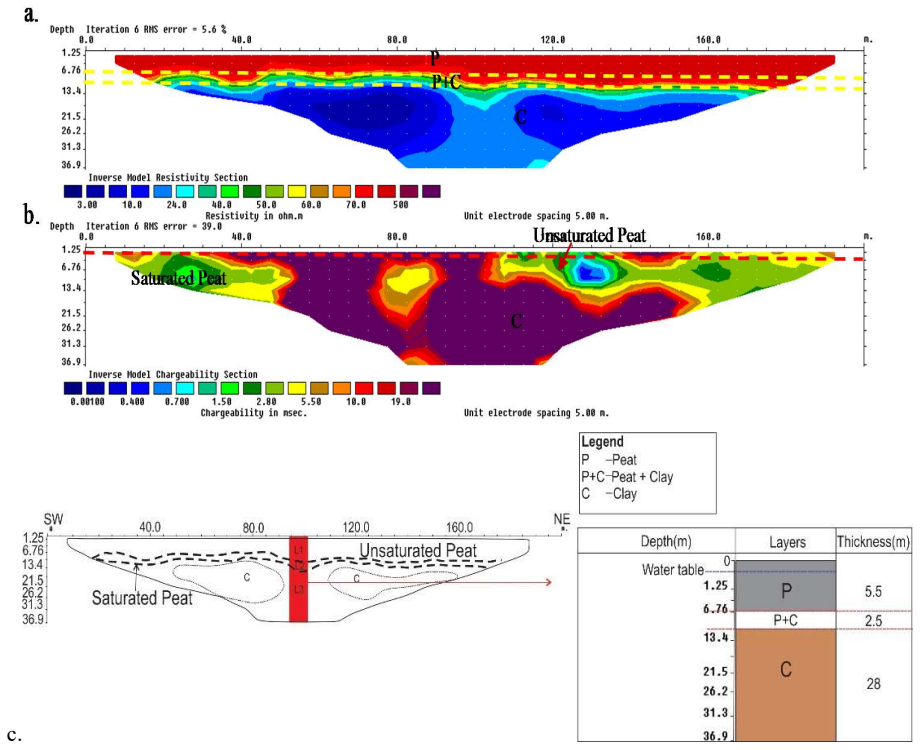
a.
P
P+C
C
Inverse Model Resistivity Section
Resistivity in ohm.m
Unit electrode spacing 5.00 m.
b.
Unsaturated Peat
Saturated Peat
C
Inverse Model Chargeability Section
Chargeability in msec.
Unit electrode spacing 5.00 m.
c.
SW
NE
Unsaturated Peat
Saturated Peat
C
Legend
P –Peat
P+C–Peat + Clay
C –Clay
Depth(m)
Layers
Thickness(m)
Water table
P
P+C
C
5.5
2.5
28

9

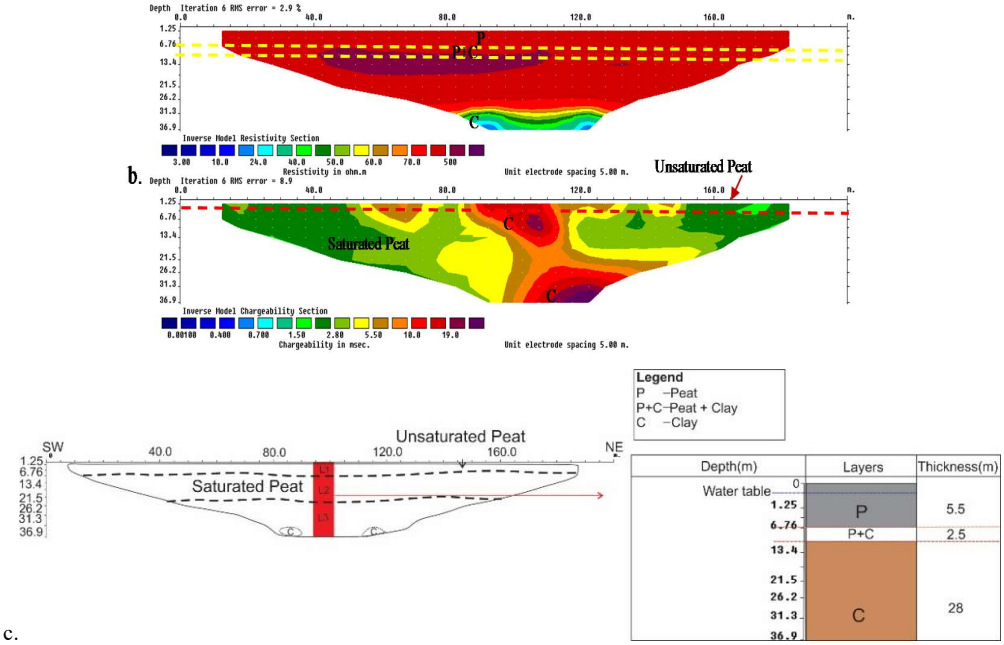

Figures 3-9. The summary of the electrical resistivity survey at Klias Peninsula. The part "c" of each figure shows the illustration of the profile.

3-2 Borehole data

Three borehole logs, BH, were observed at a variety of depths (Fig. 10). Boreholes A, B and C were taken to a depth of approximately 6 m, 1 m and 0.5 m, respectively. For BHA, the first layer reveals a peat layer at a depth of 0-5.5 m. The moisture content, organic matter and pH of peat range from 300 to 1000%, 80 to 90% and 3 to 4, respectively. The second layer at a depth of 5.5 m to 6 m is composed of a clay layer. The low organic matter (30-60)% and pH value of 5 show the presence of a clay layer at 5 m onwards (Table 2). The peat layer was revealed at a depth of 0-5 m, whereas a clay layer was identified at a depth of 5.5-6 m.

4 Discussion

4-1 Subsurface electrical resistivity modelling

The resistivity distribution of the ERT profiles reflects the resistivity model of different geological layers as shown in Figs. 3-9. For all resistivity sections, the highest resistivity value ranges from 15 Ωm to 500 Ωm and is followed by a low resistivity value ranging from 3 Ωm to 60 Ωm. Based on the correlation of resistivity models and borehole data, three types of distinct layers were obtained and classified as low resistivity (3-60 Ωm), intermediate resistivity (20-80 Ωm) and high resistivity (60-500 Ωm). The first layer indicates the peat layer with a high resistivity value at depth of 0-5.5 m and the second layer represents the boundary between peat and marine clay with an intermediate resistivity value at depth of 5.5 m. The third layer is clay layer with a low resistivity value at depth of 5.5-6 m.

Table 2. The physicochemical properties of borehole data at Klias Peninsula, Beaufort, Sabah.

Depth (m)	pH			Organic Matter (OM) (%)			Moisture Content (%)		
	BHA	BHB	BHC	BHA	BHB	BHC	BHA	BHB	BHC
0.0	-	3.66	4.49	-	99.14	100	-	331.03	334.82
0.3	-	3.67	4.53	-	98.99	100	-	455.56	412.37
0.5	4.25	3.68	4.47	82.5	98.67	77.50	1150	566.67	585.90
1.0	4.23	3.68	-	92.2	98.67	-	455.55	566.50	-
1.5	4.25	-	-	80	-	-	1328.57	-	-
2.0	4.41	-	-	72.54	-	-	880.39	-	-
2.5	4.36	-	-	74.28	-	-	880.39	-	-
3.0	4.30	-	-	34.04	-	-	963.82	-	-
3.5	4.49	-	-	81.81	-	-	1036.36	-	-
4.0	4.45	-	-	77.5	-	-	1150	-	-
4.5	4.94	-	-	30	-	-	1150	-	-
5.0	5.45	-	-	33.92	-	-	792.85	-	-
6.0	5.77	-	-	90.62	-	-	681.25	-	-
Mean	4.62	3.67	4.50	68.13	98.86	92.5	951.74	479.94	444.36
Min	4.23	3.66	4.47	30	98.67	77.50	681.25	331.03	334.82
Max	5.77	3.68	4.53	92.2	99.14	100	1328.57	566.67	585.90

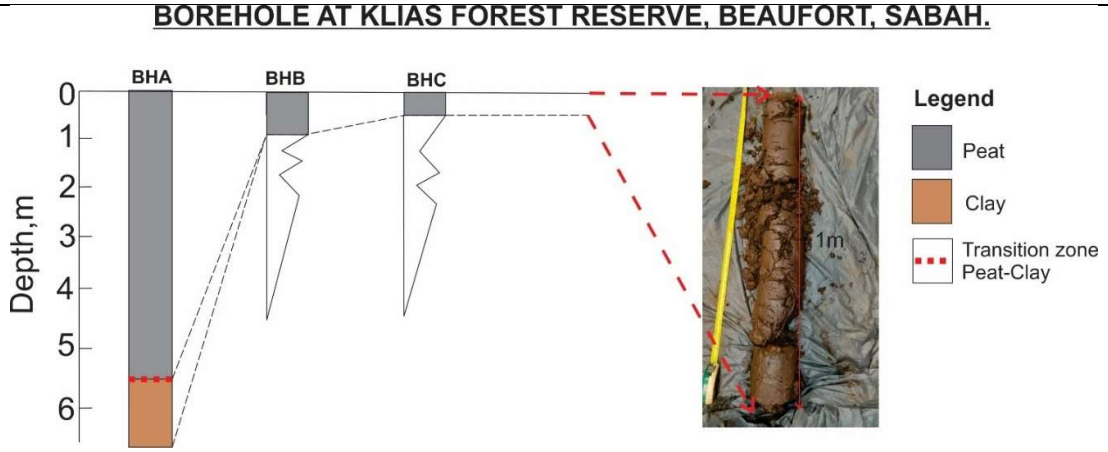

Figure 10. The borehole at Klias Peninsula, Beaufort, Sabah. The locations of these boreholes were shown in Fig. 1.

4-1-1 Resistivity characterization of peat

The uppermost deposits (P) are characterized by high resistivity values between 15 Ωm and 500 Ωm at depths of 0-5.5 m. The lithological units are known as peat material by using Schlumberger and Wenner arrays. The obtained values in this study are comparable with resistivity values of 6.7-140 Ωm of Comas et al. (2015) and the resistivity values of 6.91-93.6 Ωm of Alagbe and Faleye (2020). Based on the correlations of boreholes A, B, and C at depths 0-5.5 m, the layers are dominated by the peat layer (Fig. 10) (Table 2). The highest resistivity value of peat is 500 Ωm at resistivity lines R1, R2, R4 and R7. The lowest resistivity value for peat is 15 Ωm at resistivity line R2.

The factors of fluctuating water table on decomposition reaction and moisture content affect the resistivity value (Ponziani, 2011). The highest resistivity in lines, because of lowering the water table (1.5 m), may affect the moisture content and decomposition rate in the unsaturated zone. In correlation with the direct method, borehole data A and C in resistivity lines R1, R2, R4 and R7, the layer at depths 0-0.5 m represents the unsaturated zone that could not conduct water contributing to high resistivity. This can be supported by the finding results showing low moisture content obtained in Boreholes A and C ranging from 300% to 1000% with high

resistivity value in peat. According to Jassey et al. (2011), the space in the unsaturated peat zone is actively exposed to the oxidation process and less water retains in the peat. Kim et al. (2021) highlighted that water table fluctuation induces drier conditions and enhances the decomposition rate. Lowering the water table leads to plenty of oxygen-filled space above the water table which activates microbial activities (Kimberly et al., 2015). In contrast, Huat et al. (2014) stated high organic content and low decomposition rate cause the resistivity value to increase. Therefore, lowering the water table influences to the moisture content, decomposition rate and high resistivity value.

The lowest resistivity value in line R2 was governed by the high water content and decomposed peat in the saturated peat zone. The material of fabric peat at the uppermost of the layer contributes to the increasing degree of decomposition and water content causes the resistivity to decrease with depth (Zainorabidin and Mohamad, 2016a). This is reasonable considering that water is a good electrical conductor and the conductivity of peat pore water increases with depth (El-Galladi, 2007). Afshin and Bujang (2009) highlighted that the resistivity of peat declines with increasing degrees of decomposition, water content and temperature. In contrast, less decomposed peat soils store more moisture during the rainy season and hold less moisture during the dry season (Blodau and Moore, 2002).

The unsaturated zone shows the highest resistivity value than the saturated zone. The resistivity value of unsaturated zone ranges from 400 Ωm to 500 Ωm while for the saturated zone it ranges from 40 Ωm to 500 Ωm. Owing to undrained peat bogs dominated in the area supported by the high moisture content, the appearance of the saturated zone in the Beaufort area ranging from 400% to 985% shows the area is occupied with waterlogged peat (Zainorabidin and Mohamad, 2016b). This can be confirmed by the high value of IP and electrical conductivity in the saturated zone ranging from 1 to 9 msec. As stated by Ponziani (2011), the electrical conductivity of peat depends on the conductivity of fluid in the saturated peat. Hence, the high value of IP shows high conductivity in the saturated zone. An unsaturated zone indicates a low IP value because peat decomposition in the unsaturated zone reduces the proportion of large pores by breaking down the plant debris into small fragments, thus reducing the inter-particle pore spaces for water conductivity (Moore et al., 2005).

4-1-2 Resistivity characterization of the transition zone

The intermediate resistivity (20-80 Ωm) was present at the transition zone of peat/clay with a depth of 6-8 m. Borehole A indicates the composition of the peat/clay layer at depth 5.5 m. In resistivity lines, R1 and R5 show a high resistivity (80 Ωm) of peat/clay, while the lowest peat/clay resistivity is 20 Ωm at resistivity line R6. Both higher and lower resistivity values for the peat/clay layer were used in the Schlumberger array. This layer represents a partially saturated zone that could conduct water to peat and clay materials. The resistivity value decreased drastically because of the presence of clay fraction (Huat et al., 2014). The clay minerals provide high Cation Exchange Capacity (CEC) which contributes to the low resistivity value.

4-1-3 Resistivity characterization of clay

The lowest resistivity (3-60 Ωm) is predominantly by clayey layer (C) at depths 8 m to 36 m in the saturated zone. The lithological units of the marine clay layer were observed at a depth of 6.0 m downwards by using borehole A. Moreover, the highest resistivity value for clay is 60 Ωm at resistivity lines R1, R2, R3, R5, R6 and R7. The lowest resistivity value for clay at

line R4 is 3 Ωm. According to the research, the resistivity of clay decreases with depths in ranges 5 Ωm to10 Ωm (Jun et al., 2017). In contrast, based on Ishola et al. (2021), the resistivity for the clay layer is 5 Ωm to 50 Ωm.

The lower resistivity value in clay is due to low organic matter, high CEC and the presence of saturated clay. According to El-Galladi (2007), downwards the depth, high decomposition of organic content leads to the contribution of high negative charges. The high cation exchange capacity provided by the clay fraction, causes drastic drops in resistivity value and high chargeability (Jakalia, 2015). This can be proven with the pH results where the value increases with the depth ranging from 4.0 to 5.0 (Table 2) at depth 5 m onwards. This is because the H+ is displaced with cation released from the decomposition of organic matter and adsorbed on the surface conductivity of clay minerals which contributes to low resistivity value (Wasis et al., 2019). Furthermore, low resistivity value is influenced by the saturated clay ranging from 2 msec to 10 msec. The high conductivity of fluid in saturated clay affects the resistivity value (Kim et al., 2011). Thus, low organic matter content, high CEC and the presence of saturated clay contribute to the low resistivity value of clay. Moreover, differences in structure, bulk density and porosity in clay minerals contribute to low resistivity value (Dahlin and Zhou, 2006). The structure and shape of clay are flat which induces the ability of water to diffuse between the minerals (Muhammad et al., 2020); hence, the surface area increases and supports the high conductivity. The appearance of clay in the study area can be confirmed based on the X-Ray diffraction where illite and kaolinite were investigated. Other than that, by the correlation with borehole data, the clay soil (2.59 g/cm^3) contains high bulk density compared to peat soil (0.09-0.27) g/cm^3. High bulk density will lead to low total porosity, compacted structure, retaining moisture, low water content released and also, less water filled in the pore spaces. Therefore, the larger the surface area, high bulk density and low porosity, the lower the resistivity value (Kurnain et al., 2002; Gnatowski et al., 2010).

In contrast, the previous research by Mohamad et al., (2021), stated low resistivity values were obtained on the marine clay layer. The clay layer in Klias Peninsula was known as marine clay because of peat deposits in the coastal area (Haider et al., 2013). The coastal area near Padas Valley contributes to saltwater flow in the soil profile. According to Mohamad et al. (2021), the resistivity value for marine clay ranges from 5 Ωm to 150 Ωm. In addition, Long et al. (2012) highlighted the salt content induces the electrical resistivity, thus low resistivity value (2 Ωm-80 Ωm).

4-2 The model thickness of peat

Electrical resistivity has been used successfully to determine peat thickness (Kurnain et al., 2002; Gnatowski et al., 2010; Basri et al., 2019; Musta et al., 2022) as shown in Fig. 11. The profile of peat deposits in both Wenner and Schlumberger shows similar results. Both arrays present a consistent thickening of peat deposits, but different exact depths of peat and clay layer. The profile depth obtained using the Schlumberger array with 1 m and 5 m electrode spacing was 14.9 m and 36.9 m, respectively, while using 2.5 m and 5 m electrode spacing in the Wenner array, it was 36.9 m.

The thickness of peat plays a role in carbon storage and is associated with greenhouse gas issues during peat fires in agricultural peatlands (Agus and Subiksa, 2008). According to Silvestri et al. (2019), the thickness of the peat obtained ranges between 0 and 7 m. It shows the same thickness as the research area (0-6 m). The thickness of the peat is influenced by the

low decomposition rate and high moisture content. It may prevent groundwater contamination. The groundwater conductivity in peatland ranging from 120 to 130 ms/cm is potentially contaminated by industrial and agricultural activities and fertilizers which contribute to the high concentration of Fe element (Menció et al., 2016). Based on the Fouad et al. (2021), an increase in adsorbent thickness led to rises in the adsorption of trace metals. The peat soil acts as a cover at the bottom of the surface to avoid contaminating groundwater by removing the iron element from the water. Thicker thickness of peat and clay as adsorbent materials results in higher absorption of trace metals into the materials and better prevention of groundwater contamination.

Based on the resistivity lines R1, R2, R3, R4, R5, R6 and R7, the peat layer shows a varied pattern from 0 to 6 m in the west-to-east direction obtained from borehole data carried out in the site (Fig. 12). The clay deposits were found at depths 8 m-36 m for 1 m and 5 m electrode spacing with thickness of 6-28 m. The resistivity lines R1, R5, R6 and R7 show the thickest clay layer which is 28 m compared to resistivity lines R2, R3 and R4 with 6-8 m thickness. The presence of the thickest clay layer in the resistivity line is a dangerous sign in geotechnical issues that potentially may affect the sinking foundation of the building, structure above the surface to collapse and cracks the foundation because of the movement of the building (Ayolabi et al., 2012; Bayowa and Olayiwola, 2015). Moreover, high conductivity ranging from 2 msec to 7 msec causes the material to expand and to lose rigidity. Thus, the geotechnical implication of these materials is not suitable for laying the foundation of engineering structures because of their poor shear strength (Oyedele and Olorode, 2010).

Overall, the clay layer is thickening towards the west to east with a thickness of about 6-28 m based on geophysical data, borehole data and observation on the field (Figs. 11 and 12), while the thickness of the peat layer is about 0-5.5 m and shows a varied pattern from west to east. Therefore, the coring method and Electrical Resistivity Imaging (ERI) were the effective methods for characterizing the physical properties of peat and thickness estimation of peat in the research area.

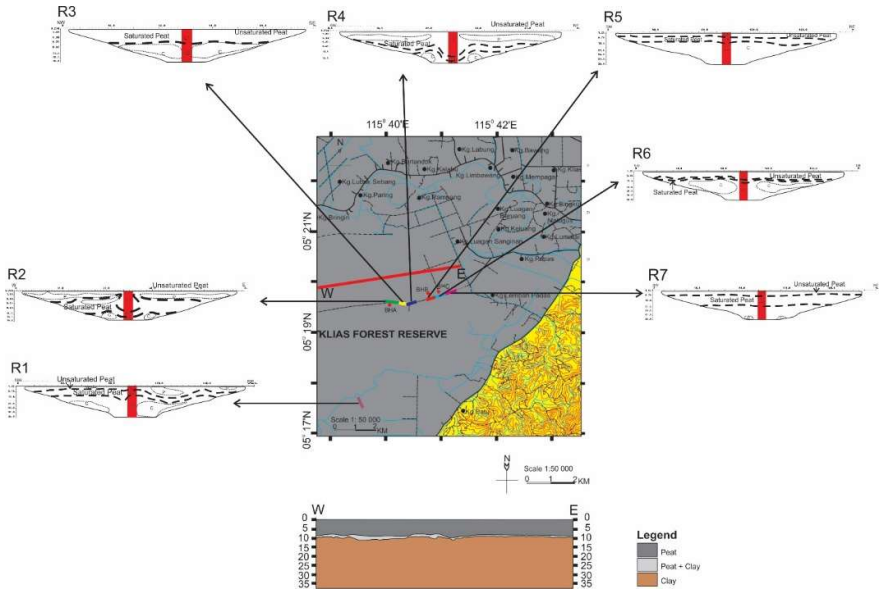

Figure 11. Interpreted geoelectrical data from R1 to R7. The lower part of the figure indicates the cross-section of the peat soil profile (W-E) at Klias Peninsula.

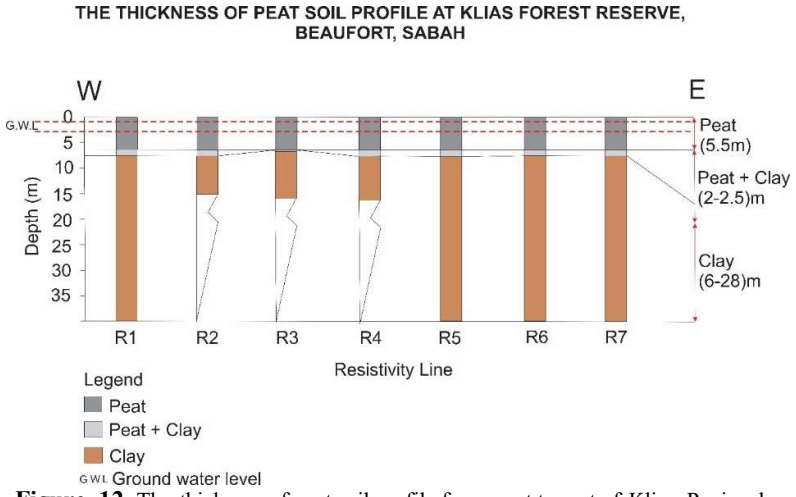

Figure 12. The thickness of peat soil profile from west to east of Klias Peninsula.

5 Conclusions

Based on the subsurface resistivity models, peat and a layer of clay were obtained and divided by the transition zone. The boundary between peat and marine clay is found at a depth of 5.5 m with a resistivity value of 20-80 Ωm. Peat is present to a depth of 5 m and is followed by a mixture of peat and clay. The clay dominated at 6 m depth. The layer of peat characterized by high resistivity values ranging from 15 Ωm to 500 Ωm and followed by low resistivity values ranging from 3 Ωm to 60 Ωm, consists predominantly of clay layer with thicknesses of 0-6 m and 6-28 m, respectively. Thus, applying ERI and core sampling was the effective method for characterizing peat physical properties and thickness estimation. Overall, the clay layer is thickening towards the west-east with a thickness of about 6-28 m, while the thickness of about 0-5.5 m for peat layer shows a varied pattern from west to east. The variety of the thickness pattern from the west-east was influenced by the fluctuation of the water table, moisture content, organic content, cation exchange capacity, bulk density and porosity.

Acknowledgements

This research was supported by University Malaysia Sabah with project code SGA0053-2019. All laboratory works have been done in the Faculty of Science and Natural Resources, University Malaysia Sabah, Kota Kinabalu, Sabah, Malaysia.

References

Afshin, A., and Bujang, B. K. H., 2009, Electrical Resistivity of Tropical Peat, Electronic Journal of Geotechnical Engineering, **14**, 1-9.

Agus, F., and Subiksa, I. G. M., 2008, Lahan Gambut: Potensi untuk Pertanian dan Aspek Lingkungan, Bogor, Indonesia: Balai Penelitian Tanah dan ICRAF.

Alagbe, O. A., and Faleye, O. E., 2020, 2D electrical resistivity imaging (ERI) for subsurface evaluation of a pre-engineering construction site in Akure, Southwestern Nigeria: International Journal of Environmental Monitoring and Analysis, **8**(2), 33-44.

Ayolabi, E. A., Folorunso, A. F., and Jegede, O. E., 2012, An application of 2D electrical resistivity tomography in geotechnical investigations of foundation defects: A case study: Journal of Geology and Mining Research, **3**, 142-151.

Basri, K., Wahab, N., Talib, M. K. A., and Zainorabidin, A., 2019, Sub-surface profiling using Electrical Resistivity

Tomography (ERT) with complement from peat sampler: Civil Engineering and Architecture, **7**, 7-18.

Bayowa, O. G., and Olayiwola, N. S., 2015, Electrical resistivity investigation for topsoil thickness, competence and corrosivity evaluation: A case study from Ladoke Akintola University of Technology, Ogbomoso, Nigeria: 2nd International Conference on Geological and Civil Engineering, **80**.

Bing, Z., and Torleif, D., 2003, Properties and effects of measurement errors on 2D resistivity imaging surveying: Near Surface Geophysics, 105-117.

Blodau, C., and Moore, T. R., 2002, Macroporosity affect water movement and pore water sampling in peat soils: Soil Science, **167**, 98-109.

Comas, X., Terry, N., Slater, L., et al., 2015, Imaging tropical peatlands in Indonesia using ground-penetrating radar (GPR) and electrical resistivity imaging (ERI): implications for carbon stock estimates and peat soil characterization: Biogeosciences, **12**, 2995–3007, https://doi.org/10.5194/bg-12-2995-2015.

Dahlin, T., and Zhou, B., 2004, A numerical comparison of 2D resistivity imaging with 10 electrode arrays: Geophysical Prospecting, **52**, 379–398.

Dahlin, T., and Zhou, B., 2006, Multiple-gradient array measurements for multichannel 2D resistivity imaging: Near Surface Geophysics, **2**, 113–123.

El-Galladi, A., 2007, Mapping peat layer using surface geoelectrical methods at Mansoura Environs, Nile Delta, Egypt: Mansoura Journal of Geology and Geophysics, **34**, 59-78.

Erica, C., Berit, V. E., Morten, F. M., et al., 2020, Investigating Lake sediments and peat deposits with geophysical methods - A case study from a kettle hole at the Late Palaeolithic site of Tyrsted, Denmark: Quaternary International, **558**, 89–106.

Gnatowski, T., Szatylowicz, J., Brandyk, T., and Kechavarzi, C., 2010, Hydraulic properties of fen peat soils in Poland: Geoderma, **154**, 188–195.

Gusti, Z., Anshari, Gusmayanti, E., and Nisa, N., 2021, The use of subsidence to estimate carbon loss from deforested and drained tropical peatlands in Indonesia: Forests, **12**, 732.

Haider, A., Erwin, O., and Gary, C., 2013, Characteristics of embedded peat in coastal environments: International Journal of Geomate, **5**(1), 610-619.

Huat, B. B. K., Prasad, A., Asadi, A., and Kazemian, S., 2014, Geotechnics of organic soils and peat: CRC Press, **41**.

Ishola, K. S., Nawawi, M. N. M., and Abdullah, K., 2014, Combining multiple electrode arrays for two-dimensional electrical resistivity imaging using the unsupervised classification technique: Pure and Applied Geophysics, **172**, 1615–1642.

Ishola, K. S., Waezuoke, C. C., and Ayolabi, E. A., 2021, Electrical resistivity imaging and multichannel analysis of surface waves for mapping the subsurface of a Wetland Area of Lagos, Nigeria: NRIAG Journal of Astronomy and Geophysics, **10**, 300–319.

Jaenicke, J., Rieley, J. O. Mott, C., Kimman, P., and Siege, F., 2008, Determination of the amount of carbon stored in Indonesian peatlands: Geoderma, **147**, 151–158.

Jakalia, 2015, Implications of soil resistivity measurements using the electrical resistivity method: A case study of a maize farm under different soil preparation modes at KNUST Agricultural Research Station, Kumasi: International Journal of Scientific & Technology Research, **4**(1), 9-18.

Jassey, V. E. J., Chiapusio, G., Gilbert, D., Buttler, A., Toussaint, M. L., and Binet, P., 2011, Experimental climate effect on seasonal variability of polyphenol. peatland water table fluctuation phenoloxidase interplay along a narrow

fen-bog ecological gradient in Sphagnum Fallax: Global Change Biology, **17**, 2945–2957.

Jun, L., Guojun, C., Songyu, L., Anand, J. P., and Haifeng, Z., 2017, Correlations between electrical resistivity and geotechnical parameters for Jiangsu marine clay using Spearman's coefficient test: International Journal of Civil Engineering, **15**, 419-429.

Kim, M., Kim, J., Kim, N., et al., 2011, Surface geophysical investigations of landslide at the Wiri area in southeastern Korea: Environmental Earth Sciences, **63**, 999-1009.

Kim, J., Rochefort, L., Alqulaiti, Z., et al., 2021, Water table fluctuation in peatlands facilitates fungal proliferation, impedes Sphagnum growth and accelerates decomposition: Frontiers in Earth Science, **8**, 1-9.

Kimberly, M. C., Lael, K. G., and Calen, C. M. T., 2015, Modelling relationships between water table depth and peat soil carbon loss in Southeast Asianplantations, Environmental Research Letters, DOI:10.1088/1748-9326/10/7/074006.

Kowalczyk, S., Żukowska, K. A., Mendecki, M. J., and Lukasiak, D., 2017, Application of electrical resistivity imaging (ERI) for the assessment of peat properties: a case study of the Całowanie Fen, Central Poland: Acta Geophysica, **65**, 223–235.

Kurnain, A., Notohadikusumo, T., Radjagukguk, B., and Sri, H., 2002, The state of decomposition of tropical peat soil under cultivated and fire-damaged peatland, in Rieley, J., and Page, S., eds.: Jakarta symposium proceedings on peatlands for people, Natural Resources Function and Sustainable Management, 168-178.

Lee, D., and Andrew, R., 2002, Investigating peatland stratigraphy and hydrogeology using integrated electrical geophysics: Geophysics, **67**, 365.

Loke, M. H., Acworth, I., and Dahlin, T., 2003, A comparison of smooth and blocky inversion methods in 2D electrical imaging surveys: Exploration Geophysics, **34**, 182–187.

Loke, M. H., Chambers, J. E., Rucker, D. F., Kuras, O., and Wilkinson, P. B., 2013, Recent developments in the direct-current geoelectrical imaging method: Journal of Applied Geophysics, **95**, 135–156.

Loke, M. H., Rucker, D. F., Chambers, J. E., Wikinson, P. B., Kuras, O., 2011, Electrical resistivity surveys and data interpretation, in Gupta, H., et al., eds., Encyclopaedia of Solid Earth Geophysics (2nd Edition): Springer-Verlag, 276-283.

Loke, M. H., 2017, RES2DINV Rapid 2-D resistivity and IP inversion using the least squares method: Geotomo Software Manual, Penang, Malaysia.

Long, M., Donohue, S., L'Heureux, J. S., et al., 2012, Relationship between electrical resistivity and basic geotechnical parameters for marine clays: Canadian Geotechnical Journal, **49**(10), 1158–1168.

Menció, A., Mas-Pla, J., Oteroc, N., et al., 2016, Nitrate pollution of groundwater: Science of the Total Environment, **539**, 241–251.

Mohamad, H. M., Kasbi, B., Baba, M., Adnan, Z., Hardianshah, S., and Ismail, S., 2021, Investigating peat soil stratigraphy and marine clay formation using the geophysical method in Padas Valley, Northern Borneo: Applied and Environmental Soil Science, 1-12.

Moharram, F., Mohamed I. G., Mahmoud H. M., and Enas, E. A., 2021, Iron (II) absorption from groundwater by natural peat soil at its in-situ conditions: Mansoura Engineering Journal, **46**, 21-27.

Moore, T. R., Trofymow, J. A., Siltanen, M., and Prescott, C., 2005, CIDET working group patterns of decomposition and carbon, nitrogen, and phosphorus dynamics of litter in upland forest and peatland sites in central Canada:

Canadian Journal of Forest Research, **35**, 133-142.

Muhammad, R. R., Acep, R., Wiyono, and Ahmad, B., 2020, Imaging tropical peatland and aquifer potential In South Sumatra using electrical resistivity tomography: Indonesian Journal of Forestry Research, **7**, 1-14.

Musta, B., Azrin Asat, M., Sin Yi, L., and Saleh, H., 2022, Geophysical investigation and geochemical study of sediment along the coastal area in Kota Belud Sabah, Malaysia: Journal of Physics, Conference Series, **2165**, 012046.

Oktanius, R. H., and Doni, P. E. P., 2016, The effectiveness of Wenner-Schlumberger and dipole-dipole array of 2D geoelectrical survey to detect the occurring of groundwater in the Gunung Kidul karst aquifer system, Yogyakarta, Indonesia: Journal of Applied Geology, **1**(2), 71–81.

Oyedele, K. F., and Olorode, D. O., 2010, Site investigations of subsurface conditions using electrical resistivity method and cone penetration test at medina estate, Gbagada, Lagos, Nigeria: World Applied Sciences Journal, **11**, 1097–1104.

Pezdir, V., Ceru, T., Horn, B., and Gosar, M., 2021, Investigating peatland stratigraphy and development of the Šijec bog (Slovenia) using near-surface geophysical methods: Catena, **206**, 1-15.

Phua, M. H., Conrad, O., Uni Kamlun, K., and Fisher, M., 2008, Multitemporal fragmentation analysis of peat swamp forest in the Klias Peninsula, Sabah, Malaysia using GIS and remote sensing: Hamburg's contribution to physical geography and landscape ecology, University of Hamburg, Hamburg, 81-90.

Ponziani, M., 2011, Influence of water content on the electrical conductivity of peat: International Water Technology Journal (IWTJ), **1**, 14-21.

Saleh, H. B., and Samsudin, A. R., 2013a, Application of vertical electrical sounding (VES) in subsurface geological investigation for potential aquifer in Lahad Datu, Sabah: AIP Conference Proceedings, 2013, 1571, 432–437.

Saleh, H. B., and Samsudin, A. R., 2013b, Substratum assessment of ganduman formation, in dent peninsular, Sabah based on geo-electrical resistivity data for identifying layer of aquifer potential: Electronic Journal of Geotechnical Engineering, **19J**, 2209-2218.

Silvestri, S., Knight, R., and Viezzoli, A., 2019, Quantification of peat thickness and stored carbon at the landscape scale in tropical peatlands: a comparison of airborne geophysics and an empirical topographic method: Journal of Geophysical Research: Earth Surface, **124**(12), 3107–3123.

Tao, Z., Songyu, L., and Guojun, C., 2018 Correlations between electrical resistivity and basic engineering property parameters for marine clays in Jiangsu, China: Journal of AppliedGeophysics, **159**, 640–648.

Wasis, B., Saharjo, B. H., and Putra, E. I., 2019, Impacts of peat fire on soil flora and fauna, soil properties and environmental damage in Riau Province, Indonesia: Biodiversities Journal of Biological Diversity, **20**(6), 70-75.

Yule, C. M., Lim, Y. Y., and Lim, T. Y., 2016, Degradation of tropical Malaysian peatlands decreases levels of phenolics in soil and in leaves of Macaranga pruinose: Frontiers in Earth Science, **4**, id45.

Yule, C. M., Lim, Y. Y., and Lim, T. Y., 2018, Recycling of phenolic compounds in Borneo's tropical peat swamp forests: Carbon Balance and Management, **55**.

Yusa, M., Sutikno, S., Lita, D., et al., 2019, Resistivity and physical characteristic of Meranti's Peat: Journal of Physics, Conference Series, **1351**, 1-6.

Yusa, M., Yamamoto, K., Koyama, A., Sutikno, S., Fatnanta, F., Fauzi, M., and

Nasrul, B., 2021, Geotechnical characterization of Bengkalis' peat using portable tools: International Journal of Geomate, **20**, 113-120.

Zainorabidin, A., and Mohamad, H. M., 2016a, Geotechnical exploration of Sabah peat soil: Engineering classifications and field survey: Electronic Journal of Geotechnical Engineering, **21**, 6671-6685.

Zainorabidin, A., and Mohamad, H. M., 2016b, Preliminary peat surveys in ecoregion delineation of North Borneo: engineering perspective: Electronic Journal of Geotechnical Engineering, **21**(12**)**, 4485–4493.

Zamri, S. N. M., Saleh, H., and Musta, B., 2022, Geochemical distribution of heavy metals in peat soil profile and estimation of water table patterns in peatland at Klias Peninsular, Sabah: Journal of Physics: Conference Series, **2314** (1), 012024.